ARTICLE IN PRESS

npj Computational Materials

https://doi.org/10.1038/s41524-026-02028-7

Article in Press

The dual role of 90° domain walls in ferroelectric switching of $Hf_{0.5}Zr_{0.5}O_2$ thin films: Insights from phase-field simulations

Received: 29 November 2025

Accepted: 22 February 2026

Cite this article as: Wen, S., Peng, R.-C., Cheng, X. *et al.* The dual role of 90° domain walls in ferroelectric switching of $Hf_{0.5}Zr_{0.5}O_2$ thin films: Insights from phase-field simulations. *npj Comput Mater* (2026). https://doi.org/10.1038/s41524-026-02028-7

Shubin Wen, Ren-Ci Peng, Xiaoxing Cheng, Min Liao & Yichun Zhou

We are providing an unedited version of this manuscript to give early access to its findings. Before final publication, the manuscript will undergo further editing. Please note there may be errors present which affect the content, and all legal disclaimers apply.

If this paper is publishing under a Transparent Peer Review model then Peer Review reports will publish with the final article.

ARTICLE IN PRESS

© The Author(s) 2026. **Open Access** This article is licensed under a Creative Commons Attribution-NonCommercial-NoDerivatives 4.0 International License, which permits any non-commercial use, sharing, distribution and reproduction in any medium or format, as long as you give appropriate credit to the original author(s) and the source, provide a link to the Creative Commons licence, and indicate if you modified the licensed material. You do not have permission under this licence to share adapted material derived from this article or parts of it. The images or other third party material in this article are included in the article's Creative Commons licence, unless indicated otherwise in a credit line to the material. If material is not included in the article's Creative Commons licence and your intended use is not permitted by statutory regulation or exceeds the permitted use, you will need to obtain permission directly from the copyright holder. To view a copy of this licence, visit http://creativecommons.org/licenses/by-nc-nd/4.0/.

ARTICLE IN PRESS

The dual role of 90° domain walls in ferroelectric switching of $Hf_{0.5}Zr_{0.5}O_2$ thin films: Insights from phase-field simulations

Shubin Wen[a], Ren-Ci Peng[a,b*], Xiaoxing Cheng[c], Min Liao[a,b*], Yichun Zhou[a,b]

[a] *School of Advanced Materials and Nanotechnology, Xidian University, Xi'an 710126, China*

[b] *Shannxi Key Laboratory of High-Orbits-Electron Materials and Protection Technology for Aerospace (HMP), Xidian University, Xi'an 710126, China*

[c] *Shenzhen International Center for Industrial and Applied Mathematics, Shenzhen Research Institute of Big Data, Shenzhen 518172, China*

*Corresponding authors. *E-mail addresses*: pengrenci@xidian.edu.cn (R.-C. Peng), mliao@xidian.edu.cn (M. Liao).

ARTICLE IN PRESS

ABSTRACT

The dynamic behavior of ferroelectric domain walls (DWs), particularly both 90° and 180° DWs, is crucial for high-performance HfO_2-based ferroelectric devices. However, fundamentally understanding DW dynamics is challenging because the role of 90° DWs and their interplay with 180° DWs in ferroelectric switching remains elusive in HfO_2-based ferroelectrics. Here, we employ phase-field simulations to investigate the dynamics of domain and DW in epitaxial $Hf_{0.5}Zr_{0.5}O_2$ thin films with the coexistence of 90° and 180° DWs. It indicates that the threshold voltage for 90° DW migration is much higher than that for 180° DW owing to the higher migration

ARTICLE IN PRESS

energy barrier for the former. 90° DWs play a complex dual role in ferroelectric switching: they lower the nucleation voltage by serving as preferential nucleation sites for 180° domain switching, while simultaneously impede the propagation of 180° DWs due to their high migration energy barrier. Furthermore, 90° DWs guide the switching pathway of nascent 180° domains around ferroelastic domains to avoid the formation of unstable charged DWs. These findings provide a fundamental mesoscale understanding of competitive and synergistic mechanisms between 90° and 180° DWs in ferroelectric switching, offering guidance for precise manipulation of DWs to optimize the performance of HfO_2-based ferroelectric memories.

Keywords: HfO_2-based ferroelectric, 90° domain wall, Domain switching, Phase-field simulations

ARTICLE IN PRESS

INTRODUCTION

The discovery of fluorite-structured HfO_2-based ferroelectric materials[1] has significantly advanced the development of next-generation non-volatile memory technologies, such as ferroelectric random-access memory (FeRAM)[2] and ferroelectric field-effect transistors (FeFETs)[3]. Compared to perovskite ferroelectric materials, HfO_2-based ferroelectric films exhibit excellent compatibility with CMOS technology[1] and scalability down to the sub-nanometer regime[4,5], offering the potential for high-density device integration. As the dimension of ferroelectric devices is continuously scaled down, the role of ferroelectric domain walls (DWs) (namely, interfaces separating adjacent domains with different polarization orientations) and their dynamic behavior

ARTICLE IN PRESS

during ferroelectric switching has become non-negligible. This is because DWs are involved not only in the nucleation and growth of ferroelectric domains but also in determining device reliability, such as wake-up[6,7], fatigue[8,9], and imprint effects[10]. Therefore, a fundamental understanding of ferroelectric DW dynamics is essential for achieving high-performance ferroelectric memory devices.

During the phase transition from the paraelectric tetragonal (T) phase to the ferroelectric orthorhombic (O) phase in HfO_2-based films, the fourfold rotational symmetry of the T phase is broken, forming O-phase variants with equivalent symmetry along different polarization orientations[11]. To minimize both the elastic strain energy induced by phase transition and the depolarization field energy, these variants tend to spontaneously form multi-domain structures separated by 180° or 90° DWs. Most previous studies[12-17] have primarily focused on 180° DWs to elucidate the physical mechanism of polarization reversal in HfO_2-based ferroelectrics. The polarization switching behavior of HfO_2-based ferroelectrics is generally considered to follow the nucleation-limited switching (NLS) mechanism, which possibly arises from the polymorphism, polycrystallinity and many defects of thin films prepared by atomic layer deposition[18,19]. Density functional theory (DFT) calculations[5] further predicted that dipoles in the O phase are highly localized within a half-unit cell width due to flat phonon bands, leading to atomically sharp 180° DWs and scale-free domain switching behavior. Notably, the migration energy barrier of these 180° DWs is comparable to the domain nucleation barrier, which implies that the migration of the DWs is limited by its own high energy barrier. This provides a complementary explanation for the

ARTICLE IN PRESS

ARTICLE IN PRESS

experimentally observed 180° polarization switching, which is predominantly governed by the nucleation process[20-22]. Moreover, latest DFT calculations[12,23,24] confirmed that multiple low-energy-barrier migration pathways for 180° DWs exist in HfO_2-based ferroelectrics, originating from the formation of 180° topological DWs during migration. This indicates their potential important contribution to polarization switching. Although 180° DWs are critical for polarization reversal, growing evidence[7,25] indicates that 90° DWs also exert a non-negligible influence on ferroelectric properties and device performance.

In contrast to the relatively well-understood 180° DWs, research on 90° DWs in HfO_2-based films has not gained momentum until recently because of significant advances in fabrication and characterization techniques of high-quality HfO_2-based ferroelectric films[26,27] and developments in atomic/mesoscale theory[24,28-30]. For example, scanning transmission electron microscopy (STEM) has clearly revealed 90° ferroelastic domains and diverse 90° DW configurations in HfO_2-based ferroelectric materials doped with various elements (e.g., Y[31], Gd[32], Si[33]), as well as in $Hf_{0.5}Zr_{0.5}O_2$ solid solution[7,8]. These studies also showed electric-field-driven ferroelastic 90° switching accompanied by reorientation of the polar axis from in-plane to out-of-plane is a main mechanism for the wake-up effect (i.e., remanent polarization enhancement)[7] and the emergence of macroscopic out-of-plane ferroelectricity in HfO_2-based ferroelectrics[7,33]. Subsequently, DFT calculations[34,35] investigated the migration energy barriers of various 90° DW configurations, and found that the 90° DWs formed around the same longest axis of O phase exhibit an ultra-low migration barrier (~ 0.07 eV) owing to the negligible lattice mismatch strain associated with

ARTICLE IN PRESS

ARTICLE IN PRESS

exchanging the two shorter axes of the O phase, thereby facilitating the rapid migration of 90° DWs and electric-field induced 90° polarization switching. Furthermore, in situ STEM experiments[25] successfully visualized the migration of neutral and charged 90° DWs in $Hf_{0.5}Zr_{0.5}O_2$ films under electron beam irradiation, showing the electrically neutral 90° DWs migrate easily, while charged 90° DWs exhibit significantly reduced mobility due to higher migration energy barriers, likely causing by pinning from charged defects (e.g., oxygen vacancies) introduced during film fabrication. These observations provide important microscopic insights into wake-up and fatigue (performance degradation) phenomena in HfO_2-based films. Furthermore, a recent in situ STEM observation[36] revealed a novel 180° polarization switching mechanism via a multi-step ferroelastic 90° switching in freestanding ZrO_2 thin films, arising from a lower energy barrier than that of the direct 180° switching due to the relaxation of elastic energy mediated by the T phase as an intermediate state, which suggested a possible competitive relationship between multi-step 90° and direct 180° polarization switching during domain switching. These studies highlight the important and complex influence of 90° DWs on domain dynamics, but the role of 90° DWs and their interplay with 180° DWs in ferroelectric switching remains elusive in HfO_2-based ferroelectrics. Thus, investigating the dynamics of 90° DWs under an external electric field is necessary for understanding the role of DWs on domain dynamics and device reliability. Notably, the coexistence of 90° and 180° DWs was observed in HfO_2-based films[37], but there exist major difficulties in not only in situ experimental characterization of shift of oxygen atom due to its small atomic number and the subsequent dynamics of such mixed DW configurations under in situ

ARTICLE IN PRESS

external electric field but also the inability of DFT to meet the computational requirements for the above dynamics at both large spatial scale and long temporal scale. Therefore, it remains challenging to gain a comprehensive understanding of domain dynamics under such mixed domain-wall configurations and the potential complex interplay between 90° and 180° DWs during the ferroelectric domain switching.

In this work, we systematically investigate the domain evolution and DW motion in epitaxial $Hf_{0.5}Zr_{0.5}O_2$ (HZO) thin films with the coexistence of 90° and 180° DW configurations under the applied voltages using phase-field simulations. The results demonstrate that the migration behaviors of 90° and 180° DWs exhibit distinct voltage dependence, which originates from their different migration energy barriers. Additionally, 90° DWs act as preferential nucleation sites for 180° domain switching, effectively reducing the nucleation voltage, but simultaneously hinder the lateral growth of 180° domains. Furthermore, the local ferroelectric switching simulated around the 90° DWs under a Lorentz-like probe voltage indicates that the switching pathway of nascent 180° domains is guided by 90° DWs, which avoids the formation of high-energy charged DWs. These findings reveal the competitive and synergistic mechanisms between 90° and 180° DWs in ferroelectric switching, providing critical insights into experimental precise manipulation of DWs for next-generation HfO_2-based ferroelectric devices with high performance and robust reliability.

ARTICLE IN PRESS

RESULTS

DW configurations and model validation

ARTICLE IN PRESS

Figure 1a illustrates the possible crystallographic orientation relationships between the (010)-oriented T paraelectric phase and the ferroelectric O phase. The parent T phase possesses a longer c_T axis and a shorter a_T axis, while the lattice parameters of the product O phase satisfy $a_O > c_O > b_O$, with the c_O axis being the polar axis. To minimize the elastic energy generated by lattice mismatch during the T-O phase transformation, the c_T axis exhibits a tendency to transform into the a_O axis, whereas the a_T axis transforms into either the c_O axis or the b_O axis with an equal probability based on symmetry considerations, resulting in four possible orthorhombic variants as shown in Figure 1a. We define regions with the same polarization direction as ferroelectric domains: *b* domains denote regions where the polar axis is parallel to the *y* direction, and *c* domains refer to regions where the polar axis is parallel to the *z* direction. Thus, the O_1, O_2, O_3, and O_4 variants correspond to the *c*+, *c*-, *b*+, and *b*- domains, respectively.

Figure 1b presents the landscape of the free energy density for polarization components (P_2, P_3) in the HZO thin film. The landscape exhibits four degenerate energy minima located at ($P_2 = \pm P_s$, $P_3 = 0$) and ($P_2 = 0$, $P_3 = \pm P_s$) (see Supplementary Fig. 1), corresponding to the *b*+/*b*- and *c*+/*c*- domains, respectively, where P_s denotes the spontaneous polarization. This result indicates that the four orthorhombic variants have equal thermodynamic probabilities of formation under the uniaxial strain $\varepsilon_{11} = 0.03$. The reason for selecting the specific strain value of $\varepsilon_{11} = 0.03$ is that this critical strain value is intended to render the energy barrier for the T-to-O phase transition zero, thereby enabling a phase-pure O-phase structure in the simulations. This configuration serves as the initial state required for our study. Furthermore, this strain value falls within a typical range (≤

ARTICLE IN PRESS

ARTICLE IN PRESS

3.5%) achievable in experiments[38]. Accordingly, it is selected as a representative strain value for the simulations. Starting from a random initial polarization configuration, stable domain structures are obtained via phase-field simulations, as shown in Fig. 1c. The simulated domain morphology demonstrates the coexistence of all four variants, consistent with the predictions of the thermodynamic potential and in good agreement with experimental observations[33]. According to previous reports, one type of 90° DW formed between the O_1 (O_2) and O_3 (O_4) variants along the *y* direction is a hard DW[34,39], while the two types of 180° DWs formed between the O_1 and O_2 variants along the *x* and *y* directions (or those formed between the O_3 and O_4 variants along the *x* and *z* directions) are classified as soft and hard DWs[40,41], respectively. Here, soft DW implies that the change in polarization is gradual at the DW, while hard DW indicates that the variation of polarization is abrupt at the DW[40,41]. Soft and hard DWs have been theoretically predicted by DFT calculations[36], while hard DWs have been directly confirmed via high-resolution TEM techniques[42] and recent indirect experimental evidence strongly suggests the possible existence of soft DWs, such as hysteresis-free negative capacitance[43,44] and switching behaviors limited by DW motion[45] in HfO_2-based ferroelectric films. Other DW configurations[34] are possible but are excluded from consideration due to their energetic instability caused by electrostatic or elastic incompatibility[46]. Additionally, the *P*-*E* loop is calculated in Fig. 1d, from which the remanent polarization (P_r) is 29 μC/cm^2 and the coercive field (E_c) is 1.2 MV/cm, both falling within the typical range of electric properties (10-30 μC/cm^2 for P_r and 1-2 MV/cm for E_c) reported

ARTICLE IN PRESS

ARTICLE IN PRESS

experimentally for HZO films[47]. These results collectively demonstrate good reliability of the constructed thermodynamic potential and the phase-field model.

Ferroelectric switching in the HZO films

To investigate the influence of 90° and 180° DWs on ferroelectric switching in the HZO films under the applied voltage, a cubic *c*- domain nucleus of 10 nm × 10 nm × 10 nm and a thermodynamically stable stripe-like *b*- domain nucleus of 128 nm × 10 nm × 10 nm (here, 90° DWs are formed with 45° orientation angles relative to the *y* axis) are embedded within the initial *c*+ domain. Notably, the length of the stripe is the same as the dimension of the matrix domain in the model. This domain configuration is relaxed to equilibrium under zero applied voltage, as shown in Fig. 2a. The chosen configuration is designed to introduce both 90° DWs and two types of 180° DWs (soft and hard DWs) simultaneously into the film, in order to study the influence of pre-existing 90° and 180° DWs on subsequent switching dynamics and their interaction mechanisms after nucleation has occurred; thus, the initial nucleation stage is not explicitly included. It should be noted that for an initial single-domain state without pre-introduced 90° and 180° DWs, the polarization reversal mechanism follows the NLS mechanism, as shown in Supplementary Fig. 2. A global voltage is applied to the top surface of the film to drive 180° domain switching, with the voltage increased incrementally from 0 V to 2.1 V in steps of 0.1 V. The domain structure reaches an equilibrium state under each applied voltage.

ARTICLE IN PRESS

ARTICLE IN PRESS

The evolution of *c*- domains with increasing voltage exhibits four distinct stages. Initially, as the voltage increases from 0.6 V to 0.7 V in Fig. 2b and 2c, the *c*- domain expands along the *x* direction, forming a stripe-like domain structure (Fig. 2c). This process is governed by the migration of the soft 180° DW along the *x* direction (where the DW direction refers to its normal direction), and the detailed dynamic evolution processes are shown in Supplementary Fig. 3. Subsequently, the domain structure remains stable until the voltage reaches 1.0 V (Fig. 2d). Upon further increasing the voltage to 1.1 V, nucleation and growth of 180° domains mediated by 90° DWs occur. The *c*+ domains surrounding the *b*- domain are switched to *c*- domains, leading to a further increase in the volume fraction of *c*- domains in Fig. 2e (the details discussed later). When the voltage reaches the coercive voltage of 1.2 V, the remnant *c*+ domain region is completely switched to *c*- domain in Fig. 2f (the detailed evolution illustrated in Supplementary Fig. 4), resulting from the migration of the hard 180° DW along the *y* direction. This result indicates that the critical voltage (1.2 V) for the activation of the hard 180° DW migration is significantly larger than that (0.7 V) for soft 180° DW migration, which is consistent with the previous report[40,41].

Notably, the *b*- domain persists throughout the entire process despite a decrease in its volume fraction. When the voltage is increased further to the threshold of 2.1 V for 90° DW migration, the migration of the DWs is initiated. Ultimately, the *b*- domain region is gradually occupied by the *c*- domain, resulting in the complete switching to a homogeneous *c*- domain state (see Supplementary Fig. 5). Although the 90° DWs are considered as hard DWs in our simulations and possess the same gradient coefficient of 180° hard DWs, there is a substantial difference in their threshold

ARTICLE IN PRESS

ARTICLE IN PRESS

voltages for migration. This difference possibly arises from the distinct underlying migration mechanisms (Supplementary Fig. 6): the 90° DW migrates via the collective rotation of polarization vectors at the DW that is consistent with the motion of Néel-type wall, whereas the 180° DW migrates through a transformation into an Ising-type wall. The results demonstrate a pronounced dynamic competition exists between 90° and 180° DWs (including both soft and hard types) during the ferroelectric switching process in HZO films. This competition manifests as distinct voltage dependencies for their migration behaviors: the soft 180° DW migrates at a relatively low voltage (0.7 V), the hard 180° DW is activated near the coercive voltage (~1.2 V), while the 90° DW requires a significantly higher threshold voltage (2.1 V) for migration. Furthermore, the 90° DW due to its high stability impedes the complete ferroelectric switching to a homogeneous single *c*- domain state, which could contribute to the wake-up and fatigue behaviors of ferroelectric devices[7].

ARTICLE IN PRESS

Role of 90° DWs in ferroelectric switching

Next, we investigate the detailed dynamic evolution of domain structure to elaborate the dynamics of 90° and 180° DWs during the ferroelectric switching in Fig. 3. After applying a voltage of 1.1 V to the initial domain configuration depicted in Fig. 3a, the domain evolution exhibits two distinct stages. First, new *c*- domains nucleate near the 90° DW in Fig. 3b, indicating that the 90° DW can act as a nucleation site for 180° domain switching. This possibly arises from ferroelastic strains and depolarization field effect at the 90° DW[48,49], resulting in an increase in

ARTICLE IN PRESS

local electrostatic energy that provides the driving force for the nucleation of the 180° domain (see Supplementary Fig. 7). Subsequently, the newly formed *c*- domains expand along the *y* direction in Figs. 3c-3e, eventually forming the stable domain configuration shown in Fig. 3f. Interestingly, the orientation of the 90° DW undergoes 90° rotation relative to the *y* axis from the initial 45° to 135° as shown in Fig. 3a and 3f during the domain evolution. Such reorientation of the 90° DW mainly results from the minimization of electrostatic energy to avoid the formation of thermodynamically unstable head-to-head or tail-to-tail charged 90° DWs with high electrostatic energy[50]. It is noteworthy that the growth of the new *c*- domains ceases after reaching a certain size, which is possibly related to a change in the type of 180° DW (i.e., from soft DW to hard DW).

To further elaborate the above origin, the distribution of the polarization component P_3 along the *y* direction is analyzed at different time steps, as displayed in Fig. 3g and 3h. At 2000 time steps, the variation of P_3 at DWs I and II is relatively gradual, with domain-wall widths of 0.74 nm and 0.96 nm, respectively, showing typical soft DW characteristics. In contrast, at 5000 time steps, the variation of P_3 at the DWs becomes abrupt, and the DW width decreases to 0.26 nm, which indeed demonstrates a transition from soft to hard DWs. Notably, DW I migrates to the right-hand side of DW II, owing to the in-plane periodic boundary conditions employed in the simulation. This suggests that the cessation of *c*- domain growth results from the gradual transformation of the DWs from a metastable soft DW to a stable hard DW during their migration along the *y* direction. Once the DWs stabilize into the hard type, a moderate applied voltage is insufficient to overcome their migration barrier, and thus DW motion halts. Hence, it reveals that

ARTICLE IN PRESS

ARTICLE IN PRESS

the nucleation-growth-stabilization process of the new *c*- domain is accompanied by the dynamic transformation of soft DWs into hard DWs, indicating that the stability of the domain structure is closely related to the properties of DW. Moreover, our simulations indicate that pre-existing 90° DWs can serve as nucleation sites, effectively promoting the formation of new 180° domains at voltages below the coercive voltage.

Quantification of the DW migration energy barrier

To elucidate the dynamic competition between 90° and 180° DWs, we perform a quantitative comparison of their migration energy barriers. First, a *b*- domain nucleus of 128 nm × 64 nm × 10 nm (90° DWs are formed with 135° orientation angles relative to the *y* axis) is embedded within the initial *c*+ domain. This domain structure is relaxed to equilibrium under zero applied voltage, as shown in the inset (i) of Fig. 4a. Subsequently, the threshold voltage (2.1 V) for 90° DW migration is applied to the top surface of the film to drive DW motion (insets (ii) and (iii) in Fig. 4a), until the film is completely transformed into a homogeneous *c*- domain state. Since the applied voltage is the primary driving force for DW migration, the intrinsic energy density ($f_{\mathrm{intrinsic}}$) is defined as the value that subtracts the electrostatic energy density from the total energy density. The evolution of $f_{\mathrm{intrinsic}}$ with time steps is shown in Fig. 4a, exhibiting two stages: (i) a rapid increase, followed by (ii) a slow increase until stabilization. The results indicate that the migration energy barrier for the 90° DW is 4.36×10^{6} J/m^{3}, which is much higher than that of the soft DW (8.24×10^{5} J/m^{3}) and the hard DW (3.38×10^{6} J/m^{3}) (see Supplementary Fig. 8). This quantitative

ARTICLE IN PRESS

ARTICLE IN PRESS

disparity in DW energy barriers fundamentally explains the distinct voltage-dependent responses of the 90° and 180° DWs observed in Fig. 2, unambiguously identifying the 90° DW as a "kinetic bottleneck" during the domain switching.

Furthermore, the temporal evolution of individual energy components and the total energy density is analyzed to reveal the underlying mechanism of the variation in $f_{\mathrm{intrinsic}}$ with time steps in Fig. 4b. The rapid increase of $f_{\mathrm{intrinsic}}$ in the first stage primarily originates from an increase in f_{Landau} that is only partially compensated by a decrease in f_{elastic}, while the change in f_{grad} is negligible. This phenomenon is attributed to the increased polarization induced by the applied electric field, which drives the polarization state away from the spontaneous polarization corresponding to the minimum of f_{Landau} and further induces a reduction in f_{elastic} indirectly through the electrostrictive effect. The slow increase in $f_{\mathrm{intrinsic}}$ during the second stage arises from ferroelastic 90° switching from *b*- domain to *c*- domain via 90° DW migration (see Supplementary Fig. 9). Hence, it demonstrates that the 90° DW migration is driven by the minimization of f_{elastic}, f_{electric}, and f_{grad}, albeit at the expense of an increase in f_{Landau}.

ARTICLE IN PRESS

Local 180° polarization switching around the 90° DWs

Finally, the detailed behavior of local 180° polarization switching around the 90° DWs is investigated to further understand ferroelectric switching pathways in the HZO thin films under a probe voltage using phase-field simulations. First, a *b*- domain nucleus of 128 nm × 10 nm × 20 nm (90° DWs oriented at 45°relative to the *y* axis) is embedded within the initial *c*+ domain, as

ARTICLE IN PRESS

shown in Fig. 5a. Then, a voltage with a Lorentz-like distribution is applied to the top surface of the film, while the bottom surface is grounded (Fig. 5a), mimicking local 180° polarization switching under a probe voltage. The spatial distribution of the applied voltage is expressed as[51]:

$$\phi_{top}(x_1,\ x_2) = \phi_0 \frac{\gamma^2}{(x_1 - x_1^0)^2 + (x_1 - x_1^0)^2 + \gamma^2} \quad (1)$$

where ϕ_0 and (x_1, x_2) represent the peak amplitude and center position of the voltage, respectively, and γ is the half-width at half-maximum of the voltage peak, set as 20 nm in the simulations. To observe domain evolution near the 90° DW, the center of the voltage (i.e., $x_1^0 = 64$ nm, $x_2^0 = 64$ nm) is positioned close to the 90° DW. Under the applied voltage, a new *c*-domain nucleates beneath the tip center in Fig. 5b, which is consistent with the previous simulation results of $Pb(Zr_{0.2}, Ti_{0.8})O_3$ (PZT) thin films[52]. Unlike the three-dimensional conical domain nuclei formed in PZT films[52], the domain nucleus in the HZO film exhibits a two-dimensional trapezoidal structure elongated along the *x* direction (see Supplementary Fig. 10). This behavior arises from the much stronger inter-domain coupling along the *x* direction (soft 180° DWs) compared to the *y* direction (hard 180° DWs)[41], which facilitates preferential expansion along the *x* direction. In the initial stage, the *c*- domain extends vertically along the thickness direction in a needle-like morphology, with negligible lateral expansion, thereby effectively suppressing the formation of bound charges at the domain boundary. When the growing *c*- domain reaches the 90° DW, its vertical growth is hindered, and it begins to expand laterally to avoid the formation of a high-energy head-to-head charged 90° DW. Notably, the nascent *c*- domain in the HZO film expands

ARTICLE IN PRESS

by directly penetrating the existing *b*- domain region and subsequently the neutral 90° DW is formed. As the *c*- domain further expands into the adjacent *c*+ domain region on the right (Fig. 5c and 5d), its growth direction turns back to vertical extension along the thickness direction to avoid the formation of 180° head-to-head DW. These results demonstrate that the 90° DW strongly inhibits the vertical growth of the *c*- domain and redirects its growth pathway during the ferroelectric switching.

ARTICLE IN PRESS

DISCUSSION

In summary, we have investigated the complex domain dynamics and the role of 90° DWs in ferroelectric switching in the epitaxial HZO thin films containing both 90° and 180° DWs under the applied voltage using phase-field simulations. The results reveal pronounced voltage-dependent migration behaviors with clear competitive interactions between 90° and 180° DWs. The threshold voltage required for 90° DWs migration (2.1 V) is significantly larger than those for soft (0.7 V) and hard (1.2 V) 180° DWs, which is attributed to the much higher migration energy barrier of 90° DWs (4.36×10^6 J/m^3) compared with soft (8.24×10^5 J/m^3) and hard (3.38×10^6 J/m^3) 180° DWs. It also reveals that the nucleation-growth-stabilization process of new domain is accompanied by the dynamic transformation of soft 180° DWs into hard 180° DWs, and the reorientation of the 90° DW that undergoes 90° rotation, which contributes to ferroelectric switching. The study further demonstrates that pre-existing 90° DWs exhibit a dual role in ferroelectric switching. On the one hand, 90° DWs act as effective preferential nucleation sites for

ARTICLE IN PRESS

180° domain switching owing to the elevated local energy nearby 90° DWs, enabling the nucleation below the coercive voltage. On the other hand, high migration energy barrier of 90° DWs makes them a kinetic bottleneck that impedes 180° DW propagation due to their high migration energy barrier, thereby hindering complete polarization reversal to a uniform single-domain state. This phenomenon possibly contributes to device characteristics such as wake-up and fatigue. Additionally, we demonstrate that 90° DWs significantly modify the ferroelectric switching pathway of nascent 180° domains around ferroelastic domains, which inhibits 180° DW vertical motion along the thickness direction and prompts domain lateral expansion to avoid the formation of charged DWs with high electrostatic energy. Overall, this study provides a fundamental understanding of the competitive and synergistic mechanisms between 90° and 180° DWs in ferroelectric switching of HfO_2-based ferroelectrics, offering guidance for the precise experimental manipulation of DW engineering in potential device applications, such as next-generation ferroelectric DW-based nanodevices with high performance and robust reliability and possible multilevel ferroelectric memory owing to their different migration barriers.

ARTICLE IN PRESS

METHODS

Phase-field model

In the phase-field model of the paraelectric-ferroelectric phase transition from the (010)-oriented T to O phase in HZO thin film[41,53], the polarization vector $\boldsymbol{P}$ is taken as the order parameter

ARTICLE IN PRESS

to describe the ferroelectric domain structure. The temporal and spatial evolution of $\boldsymbol{P}$ is given by the time-dependent Ginzburg-Landau (TDGL) equation:

$$\frac{\partial P_i(\boldsymbol{r},t)}{\partial t} = -L\frac{\delta F}{\delta P_i(\boldsymbol{r},t)}, (i=1,2,3) \quad (2)$$

where L is the kinetic coefficient, and $\boldsymbol{r}$ denotes the spatial position vector, with the x, y, and z axes corresponding to the [100], [010], and [001] crystallographic orientations of the (001)-oriented HZO thin film, respectively. F represents the total free energy of the HZO thin film, given as:

$$F = \iiint \left(f_{\text{Landau}} + f_{\text{elastic}} + f_{\text{electric}} + f_{\text{grad}} \right) \mathrm{d}V \quad (3)$$

where V is the volume of the HZO thin film, and f_{Landau}, f_{elastic}, f_{electric}, and f_{grad} represent the free energy densities of the bulk energy, elastic energy, electrostatic energy, and gradient energy, respectively. The bulk free energy density can be expanded as a sixth-order polynomial:

$$\begin{aligned} f_{\text{Landau}} &= \alpha_1\left(P_1^2+P_2^2+P_3^2\right)+\alpha_{11}\left(P_1^4+P_2^4+P_3^4\right)+\alpha_{12}\left(P_1^2P_2^2+P_2^2P_3^2+P_1^2P_3^2\right) \\ &+\alpha_{111}\left(P_1^6+P_2^6+P_3^6\right)+\alpha_{112}\left[P_1^4\left(P_2^2+P_3^2\right)+P_2^4\left(P_1^2+P_3^2\right)+P_3^4\left(P_1^2+P_2^2\right)\right] \\ &+\alpha_{123}\left(P_1^2P_2^2P_3^2\right) \end{aligned} \quad (4)$$

where α_1, α_{11}, α_{12}, α_{111}, α_{112}, and α_{123} represent the Landau coefficients. Only α_1 is temperature-dependent, expressed as $\alpha_1 = \alpha_0(T - T_0)$, where α_0 is a constant, T_0 denotes the Curie-Weiss temperature, and T represents the actual temperature, which is set as room temperature (T = 298 K) in the simulations.

The elastic energy density can be given as,

$$f_{\text{elastic}} = \frac{1}{2}C_{ijkl}e_{ij}(\boldsymbol{r})e_{kl}(\boldsymbol{r}) = \frac{1}{2}C_{ijkl}\left(\varepsilon_{ij}(\boldsymbol{r})-\varepsilon_{ij}^0(\boldsymbol{r})\right)\left(\varepsilon_{kl}(\boldsymbol{r})-\varepsilon_{kl}^0(\boldsymbol{r})\right), (i,j,k,l=1,2,3) \quad (5)$$

ARTICLE IN PRESS

where C_{ijkl} is the elastic stiffness coefficient, $e_{ij}(\boldsymbol{r})$ is the elastic strain, $\varepsilon_{ij}(\boldsymbol{r})$ represents the total strain, and $\varepsilon_{ij}^{0}(\boldsymbol{r})$ denotes the spontaneous strain. The spontaneous strain $\varepsilon_{ij}^{0}(\boldsymbol{r})$, originating from the electrostrictive effect induced by spontaneous polarization in ferroelectrics, can be calculated by $\varepsilon_{ij}^{0}(\boldsymbol{r}) = Q_{ijkl} P_i(\boldsymbol{r}) P_j(\boldsymbol{r})$, where Q_{ijkl} is the electrostrictive coefficient. Based on the Khachaturyan's theory of microelasticity[54], the total strain $\varepsilon_{ij}(\boldsymbol{r})$ is defined as the sum of homogeneous strain $\bar{\varepsilon}_{ij}$ and inhomogeneous strain $\eta_{ij}(\boldsymbol{r})$. The homogeneous strain $\bar{\varepsilon}_{ij}$ arises from the mismatch between the HZO thin film and the substrate or electrodes. The inhomogeneous strain $\eta_{ij}(\boldsymbol{r})$ is local deformations satisfying $\int \eta_{ij}(\boldsymbol{r})\,\mathrm{d}V = 0$ and can be described by $\eta_{ij}(\boldsymbol{r}) = \frac{1}{2}\left[\partial u_i(\boldsymbol{r})/\partial x_j + \partial u_j(\boldsymbol{r})/\partial x_i\right]$, where $u_i(\boldsymbol{r})$ is the displacement component. Both the spontaneous strain and total strain are defined with respect to the (010)-oriented T phase, as detailed in previous literature[53]. Given a homogeneous strain $\bar{\varepsilon}_{ij}$, the inhomogeneous strain $\eta_{ij}(\boldsymbol{r})$ can be calculated from the mechanical equilibrium equation $\sigma_{ij,j}(\boldsymbol{r}) = \partial\left[c_{ijkl}\left(\varepsilon_{kl}(\boldsymbol{r}) - \varepsilon_{kl}^{0}(\boldsymbol{r})\right)\right]/\partial x_j = 0$ using the spectral iterative method. Stress-free boundary conditions and constant applied strain conditions are applied to the top and bottom surfaces of the film, respectively. Additionally, periodic boundary conditions are employed in the in-plane directions.

The electrostatic energy density is given by

$$f_{\text{electric}} = -P_i(\boldsymbol{r})E_i(\boldsymbol{r}) - \frac{1}{2}\varepsilon_0 \kappa_{ij} E_i(\boldsymbol{r}) E_j(\boldsymbol{r}), \ (i, j = 1,2,3) \tag{6}$$

ARTICLE IN PRESS

ARTICLE IN PRESS

where ε_0 represents the vacuum permittivity, and κ_{ij} denotes the background dielectric constant, which is assumed to be isotropic for simplicity. The electric field component E_i is obtained by solving the electrostatic equilibrium equation $\partial(\varepsilon_0\kappa_{ij}E_j(\boldsymbol{r}) + P_i(\boldsymbol{r}))/\partial x_i = 0$ using the spectral iterative method. Here, the short-circuit boundary conditions are applied to solve the electrostatic equilibrium equation because the epitaxial HZO film is grown on the conducting bottom electrode and the overlaying top electrode, and hence in this case the influence of the depolarization field and bound charges can be neglected. This short-circuit boundary conditions are applicable in scenarios where the depolarization field is relatively weak or effectively screened, including (i) relatively thick ferroelectric films (> 20 nm), and (ii) ultra-thin films with ideal metal/ferroelectric interfaces where interfacial charge injection or a high density of interface defects effectively compensates the depolarization field. We will investigate the depolarization field effect on domain switching in the following work.

Furthermore, the inhomogeneous distribution of polarization in the HZO thin film gives rise to an additional free energy, denoted as the gradient energy. The anisotropic gradient energy density in the (001)-oriented HZO thin film can be expressed as:

$$\begin{aligned} f_{\text{grad}} = &\frac{1}{2}[G_{33}P_{1,1}^2 + G_{11}(P_{2,2}^2 + P_{3,3}^2)] + [(G_{13}+G_{44})P_{1,1}P_{2,2} + (G_{12}+G_{66})P_{2,2}P_{3,3} \\ &+ (G_{13}+G_{44})P_{1,1}P_{3,3}] + \frac{1}{2}[G_{44}(P_{1,2}^2 + P_{2,1}^2 + P_{1,3}^2 + P_{3,1}^2) + G_{66}(P_{2,3}^2 + P_{3,2}^2)] \end{aligned} \quad (7)$$

where G_{ij} are the gradient coefficients related to dipolar interactions at DWs. According to our previous phase-field model[41], G_{11} and G_{33} are associated with 90° DWs, G_{44} and G_{66} with 180° DWs, while $G_{13} + G_{44}$ and $G_{12} + G_{66}$ represent higher-order cross terms that can be neglected[55].

ARTICLE IN PRESS

ARTICLE IN PRESS

Since the transformation of the long axis along the x direction in the (010)-oriented T phase into the polar axis (namely, middle axis) of the O phase is energetically unfavorable, the polarization component along the x direction, P_1, is equal to 0, resulting in $P_{1,1} = P_{1,2} = P_{1,3} = 0$. This implies that the energy term $G_{33}P_{1,1}^2$ is also 0. Therefore, the independent gradient coefficients are G_{11}, G_{44}, and G_{66}. Based on DFT calculations[40] and our previous phase-field work[41], the values of the DW gradient coefficients are determined as $G_{11} = 1.1 \times 10^{-12}$ V·m^3·C^{-1}, $G_{44} = 6.8 \times 10^{-11}$ V·m^3·C^{-1}, and $G_{66} = 1.1 \times 10^{-12}$ V·m^3·C^{-1}.

To simulate the influence of 90° DWs on domain evolution in HZO thin films, a 3D discretized grid of dimensions $128\Delta x \times 128\Delta y \times 26\Delta z$ with a real-space resolution of $\Delta x = \Delta y = \Delta z = 1$ nm is employed to describe the system. The grid is partitioned into 26 layers along the z axis, with the bottom 12 layers designated as the substrate, the middle 10 layers as the HZO thin film, and the top 4 layers as the air layer. The material parameters of HZO film used in the simulations are listed in Table 1. It should be noted that the Landau coefficients are derived from fitting experimental data, the background dielectric constant is taken directly from experiments, and the gradient coefficients, the elastic stiffness coefficients, and the electrostrictive coefficients are obtained from first-principles calculations.

Table 1 Material parameters of the HZO film.

Parameter	Value	Unit
α_0	6.88465×10^5	m^2 N C^{-2}

ARTICLE IN PRESS

α_{11}	-7.40799×10^{9}	m^6 N C^{-4}
α_{12}	-5.73558×10^{7}	m^6 N C^{-4}
α_{111}	5.86933×10^{9}	m^{10} N C^{-6}
α_{112}	5.86933×10^{10}	m^{10} N C^{-6}
α_{123}	5.86933×10^{10}	m^{10} N C^{-6}
c_{11}	4.50129×10^{11}	Pa
c_{12}	1.24003×10^{11}	Pa
c_{13}	5.6152×10^{10}	Pa
c_{33}	2.69001×10^{11}	Pa
c_{44}	5.469×10^{9}	Pa
c_{66}	6.531×10^{10}	Pa
Q_{11}	0.0106	m^4 C^{-2}
Q_{12}	−0.0059	m^4 C^{-2}
Q_{13}	0.01753	m^4 C^{-2}
Q_{33}	−0.036	m^4 C^{-2}
Q_{44}	−0.0385	m^4 C^{-2}
Q_{66}	−0.00517	m^4 C^{-2}
G_{11}	1.1×10^{-12}	V m^3 C^{-1}
G_{12}	-1.1×10^{-12}	V m^3 C^{-1}
G_{13}	-6.8×10^{-11}	V m^3 C^{-1}
G_{33}	1.1×10^{-12}	V m^3 C^{-1}
G_{44}	6.8×10^{-11}	V m^3 C^{-1}
G_{66}	1.1×10^{-12}	V m^3 C^{-1}
κ_{ii} (i = 1, 2, 3)	30	

Here, c_{mn} and Q_{mn} are the Voigt notations for the elastic stiffness coefficient C_{ijkl} and the electrostrictive coefficient Q_{ijkl}, respectively.

ARTICLE IN PRESS

ARTICLE IN PRESS

DATA AVAILABILITY

The data that support the findings of this study are available from the corresponding author upon reasonable request.

CODE AVAILABILITY

The phase-field simulations are performed using the software package Mu-PRO (www.mupro.co).

ACKNOWLEDGEMENTS

This work was supported by the National Key Research and Development Program of China (Grant No. 2024YFA1208603), the Basic Research Program of Natural Science Foundation of Shaanxi Province (Grant No. 2024JC-YBMS-417), the Scientific Research Innovation Capability Support Project for Young Faculty (Grant No. ZYGXQNJSKYCXNLZCXM-M22), State Key Laboratory of New Ceramic and Fine Processing Tsinghua University (Grant No. KFZD202302), and Xidian University Specially Funded Project for Interdisciplinary Exploration (Grant No. TZJHF202517), and Hetao Shenzhen-Hong Kong Science and Technology Innovation Cooperation Zone Project (No.HZQSWS-KCCYB-2024016).

ARTICLE IN PRESS

AUTHOR CONTRIBUTIONS

ARTICLE IN PRESS

Author contributions: R.-C.P. and M.L. conceived and supervised the project. S.W. performed the phase-field simulations. R.-C.P. and S.W. wrote the main manuscript with feedback from X.C., Y.Z. and M.L. All authors reviewed the manuscript.

COMPETING INTERESTS

The authors declare no competing financial or non-financial interests.

ARTICLE IN PRESS

REFERENCES

1. Boescke, T. S., Müller, J., Bräuhaus, D., Schröder, U. & Böttger, U. Ferroelectricity in hafnium oxide thin films. *Appl. Phys. Lett.* **99**, 102903 (2011).
2. Park, J. Y. *et al.* Revival of ferroelectric memories based on emerging fluorite-structured ferroelectrics. *Adv. Mater.* **35**, 2204904 (2023).
3. Khan, A. I., Keshavarzi, A. & Datta, S. The future of ferroelectric field-effect transistor technology. *Nat. Electron.* **3**, 588-597 (2020).
4. Cheema, S. S. *et al.* Enhanced ferroelectricity in ultrathin films grown directly on silicon. *Nature* **580**, 478-482 (2020).
5. Lee, H. J. *et al.* Scale-free ferroelectricity induced by flat phonon bands in HfO_2. *Science* **369**, 1343-1347 (2020).
6. Zhou, P. A. *et al.* Intrinsic 90° charged domain wall and its effects on ferroelectric properties. *Acta Mater.* **232**, 117920 (2022).

ARTICLE IN PRESS

7. Zhang, S. R. *et al.* Domain wall evolution in $Hf_{0.5}Zr_{0.5}O_2$ ferroelectrics under field-cycling behavior. *Research* **6**, 0093 (2023).

8. Wu, F. L. *et al.* Effects of polarization behavior on wake-up and fatigue of hafnium-based ferroelectric thin films. *Small Methods* **9**, e00865 (2025).

9. Zeng, B. J. *et al.* Polarization fatigue mechanism of laminated hafnium zirconium oxide ferroelectric thin films. *Acta Mater.* **272**, 119920 (2024).

10. Xie, M. T., Yu, H. Y., Zhang, B. H., Xu, C. S. & Xiang, H. J. Role of domain walls on imprint and fatigue in HfO_2-based ferroelectrics. *Phys. Rev. B* **111**, 184108 (2025).

11. Zhu, T. Y., Ma, L. Y., Deng, S. Q. & Liu, S. Progress in computational understanding of ferroelectric mechanisms in HfO_2. *npj Comput. Mater.* **10**, 188 (2024).

12. Choe, D. H. *et al.* Unexpectedly low barrier of ferroelectric switching in HfO_2 via topological domain walls. *Mater. Today* **50**, 8-15 (2021).

13. Zhao, G.-D., Liu, X., Ren, W., Zhu, X. & Yu, S. Symmetry of ferroelectric switching and domain walls in hafnium dioxide. *Phys. Rev. B* **106**, 064104 (2022).

14. Wu, Y. *et al.* Unconventional polarization-switching mechanism in (Hf, Zr)O_2 ferroelectrics and its implications. *Phys. Rev. Lett.* **131**, 226802 (2023).

15. Yang, J. Y. *et al.* Theoretical lower limit of coercive field in ferroelectric hafnia. *Phys. Rev. X* **15**, 021042 (2025).

16. Ye, K. H. *et al.* Ab Initio study on 3D anisotropic ferroelectric switching mechanism and coercive field in HfO_2 and ZrO_2. *Adv. Funct. Mater.*, 2500390 (2025).

ARTICLE IN PRESS

ARTICLE IN PRESS

17. Zhou, S. S. & Rappe, A. M. Nucleation mechanism of multiple-order parameter ferroelectric domain wall motion in hafnia. *P. Natl. Acad. Sci. U.S.A.* **122**, e2406316122 (2025).

18. Guido, R. *et al.* Ferroelectric $Al_{0.85}Sc_{0.15}N$ and $Hf_{0.5}Zr_{0.5}O_2$ domain switching dynamics. *ACS Appl. Mater. Interfaces* **16**, 42415-42425 (2024).

19. Guido, R. *et al.* in *Ferroelectricity in doped hafnium oxide (Second Edition)* (eds Uwe Schroeder, Cheol Seong Hwang, & Hiroshi Funakubo) Ch. 7.1 - Polarization switching in HfO_2-based devices, 545-571 (Woodhead Publishing, 2025).

20. Buragohain, P. *et al.* Effect of film microstructure on domain nucleation and intrinsic switching in ferroelectric Y:HfO_2 thin film capacitors. *Adv. Funct. Mater.* **32**, 2108876 (2022).

21. Zhou, C. *et al.* Enhanced polarization switching characteristics of HfO_2 ultrathin films via acceptor-donor co-doping. *Nat. Commun.* **15**, 2893 (2024).

22. Liu, J. T. *et al.* Ultra-low-voltage operation, large ferroelectric polarization, fast switching speed, and high endurance of 450 °C processed HZO thin films by starting-layer engineering. *J. Mater. Sci. Technol.* **241**, 311-319 (2026).

23. Zhou, S. S., Qin, S. H. & Rappe, A. M. Domain wall reactions in multiple-order parameter ferroelectrics. *Phys. Rev. Lett.* **134**, 136802 (2025).

24. Qi, Y. B., Singh, S. & Rabe, K. M. Polarization switching in ferroelectric HfO_2 from first-principles lattice mode analysis. *Phys. Rev. B* **111**, 134106 (2025).

25. Zheng, Y. Z. *et al.* Direct atomic-scale visualization of the 90° domain walls and their migrations in $Hf_{0.5}Zr_{0.5}O_2$ ferroelectric thin films. *Mater. Today Nano* **24**, 100406 (2023).

ARTICLE IN PRESS

ARTICLE IN PRESS

26. Li, X. Y. *et al.* Polarization switching and correlated phase transitions in fluorite-structure ZrO_2 nanocrystals. *Adv. Mater.* **35**, 2207736 (2023).

27. Li, X. *et al.* Ferroelastically protected reversible orthorhombic to monoclinic-like phase transition in ZrO_2 nanocrystals. *Nat. Mater.* **23**, 1077-1084 (2024).

28. Kumar, P., Gupta, D. & Lee, J. H. Negative gradient energy facilitates charged domain walls in HfO_2. *Phys. Rev. Lett.* **134**, 166101 (2025).

29. Yan, S. A. *et al.* Artificial intelligence-driven phase stability evaluation and new dopants identification of hafnium oxide-based ferroelectric materials. *npj Comput. Mater.* **11**, 2 (2025).

30. Zhang, K. N. *et al.* High-throughput phase-field simulations and machine learning of resistive switching in resistive random-access memory. *npj Comput. Mater.* **6**, 198 (2020).

31. Xu, X. H. *et al.* Kinetically stabilized ferroelectricity in bulk single-crystalline HfO_2:Y. *Nat. Mater.* **20**, 826-832 (2021).

32. Grimley, E. D., Schenk, T., Mikolajick, T., Schroeder, U. & LeBeau, J. M. Atomic structure of domain and Interphase boundaries in ferroelectric HfO_2. *Adv. Mater. Interfaces* **5**, 1701258 (2018).

33. Lederer, M. *et al.* Evidence for ferroelastic switching and nanoscopic domains in polycrystalline Si-doped hafnium oxide films. *Appl. Phys. Lett.* **123**, 022903 (2023).

34. Ding, W. T., Zhang, Y. K., Tao, L. L., Yang, Q. & Zhou, Y. C. The atomic-scale domain wall structure and motion in HfO_2-based ferroelectrics: A first-principle study. *Acta Mater.* **196**, 556-564 (2020).

ARTICLE IN PRESS

ARTICLE IN PRESS

35. Hu, Q. *et al.* Mapping of the full polarization switching pathways for HfO_2 and its implications. *P. Natl. Acad. Sci. U.S.A.* **122**, e2419685122 (2025).

36. Wang, S. Y. *et al.* Unconventional ferroelectric-ferroelastic switching mediated by non-polar phase in fluorite oxides. *Adv. Mater.* **37**, 2415131 (2025).

37. Park, K. *et al.* Atomic-scale scanning of domain network in the ferroelectric HfO_2 thin film. *ACS Nano* **18**, 26315-26326 (2024).

38. Delodovici, F., Barone, P. & Picozzi, S. Trilinear-coupling-driven ferroelectricity in HfO_2. *Phys. Rev. Mater.* **5**, 064405 (2021).

39. Kiguchi, T., Shiraishi, T., Shimizu, T., Funakubo, H. & Konno, T. J. Domain orientation relationship of orthorhombic and coexisting monoclinic phases of $YO_{1.5}$-doped HfO_2 epitaxial thin films. *Jpn. J. Appl. Phys.* **57**, 11UF16 (2018).

40. Paul, T. K., Saha, A. K. & Gupta, S. K. Direction-dependent lateral domain walls in ferroelectric hafnium zirconium oxide and their gradient energy coefficients: A first-principles study. *Adv. Electron. Mater.* **10**, 2300400 (2023).

41. Wen, S. *et al.* Dynamics of anisotropic 180° domain walls in HfO_2-based ferroelectric thin films via phase-field simulations. *Acta Mater.* **301**, 121527 (2025).

42. Cheng, Y. *et al.* Reversible transition between the polar and antipolar phases and its implications for wake-up and fatigue in HfO_2-based ferroelectric thin film. *Nat. Commun.* **13**, 645 (2022).

ARTICLE IN PRESS

ARTICLE IN PRESS

43. Hoffmann, M. *et al.* Unveiling the double-well energy landscape in a ferroelectric layer. *Nature* **565**, 464-467 (2019).

44. Jo, S. *et al.* Negative differential capacitance in ultrathin ferroelectric hafnia. *Nat. Electron.* **6**, 390-397 (2023).

45. Wei, W. *et al.* In-depth understanding of polarization switching kinetics in polycrystalline $Hf_{0.5}Zr_{0.5}O_2$ ferroelectric thin film: A transition from NLS to KAI. In *2021 IEEE International Electron Devices Meeting.* 19.1.1-19.1.4 (IEEE, 2021).

46. Marton, P., Rychetsky, I. & Hlinka, J. Domain walls of ferroelectric $BaTiO_3$ within the Ginzburg-Landau-Devonshire phenomenological model. *Phys. Rev. B* **81**, 144125 (2010).

47. Fan, Y. *et al.* Hidden structural phase transition assisted ferroelectric domain orientation engineering in $Hf_{0.5}Zr_{0.5}O_2$ films. *Nat. Commun.* **16**, 4232 (2025).

48. Roelofs, A. *et al.* Depolarizing-field-mediated 180° switching in ferroelectric thin films with 90° domains. *Appl. Phys. Lett.* **80**, 1424-1426 (2002).

49. Choudhury, S. *et al.* Effect of ferroelastic twin walls on local polarization switching: Phase-field modeling. *Appl. Phys. Lett.* **93**, 162901 (2008).

50. Ishibashi, Y. & Salje, E. Theoretical consideration on the 90° domain walls in tetragonal ferroelectrics. *Ferroelectrics* **303**, 9-13 (2004).

51. Alhada-Lahbabi, K., Deleruyelle, D. & Gautier, B. Machine learning surrogate for 3D phase-field modeling of ferroelectric tip-induced electrical switching. *npj Comput. Mater.* **10**, 197 (2024).

ARTICLE IN PRESS

52. Britson, J., Gao, P., Pan, X. Q. & Chen, L. Q. Phase field simulation of charged interface formation during ferroelectric switching. *Acta Mater.* **112**, 285-294 (2016).

53. Peng, R.-C. *et al.* Revealing the role of spacer layer in domain dynamics of $Hf_{0.5}Zr_{0.5}O_2$ thin films for ferroelectrics. *Adv. Funct. Mater.* **34**, 2403864 (2024).

54. Khachaturyan, A. G. & Shatalov, G. A. Theory of macroscopic periodicity for a phase transition in the solid state. *J. Exp. Theor. Phys.* **29**, 557-561 (1969).

55. Hlinka, J. & Marton, P. Phenomenological model of a 90° domain wall in $BaTiO_3$-type ferroelectrics. *Phys. Rev. B* **74**, 104104 (2006).

ARTICLE IN PRESS

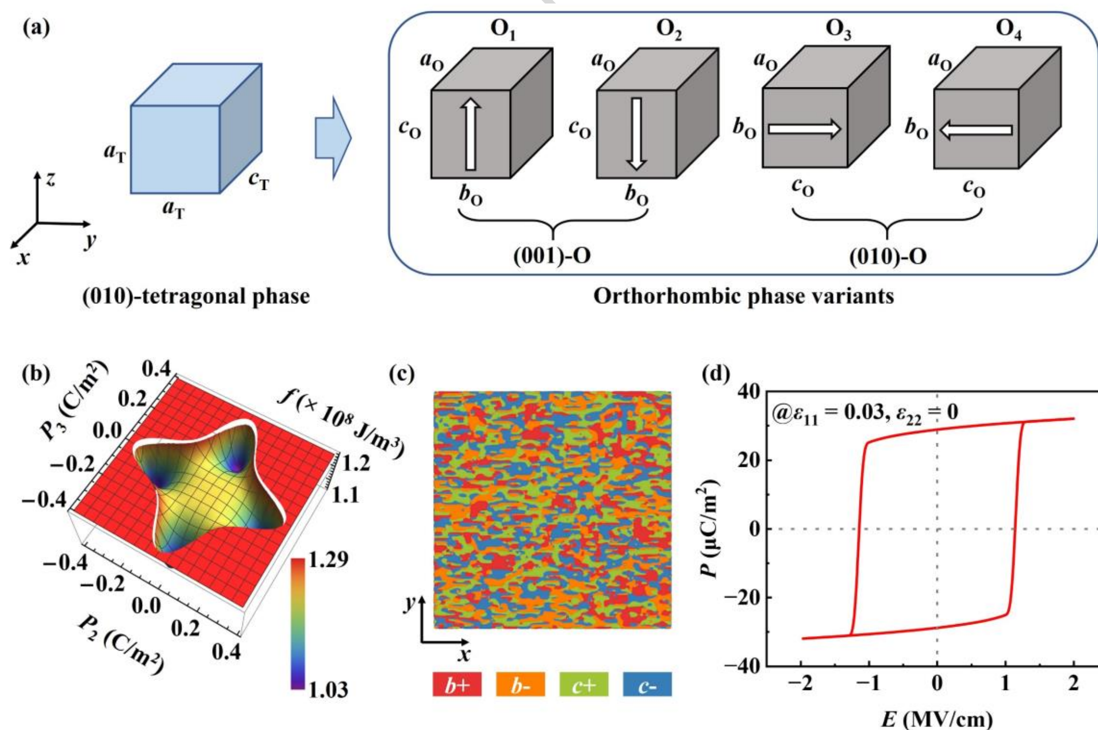

Fig. 1 | Validation of the phase-field model. a Possible variants and their corresponding relationships for the transformation from (010)-oriented paraelectric T phase to ferroelectric O

phase. The arrows indicate the spontaneous polarization directions of each variant. **b** Free energy density surface of the HZO film as a function of polarization components (P_2, P_3) under fixed strain conditions (ε_{11} = 0.03, ε_{22} = 0). **c** Stable domain structures and **d** ferroelectric hysteresis loop obtained from phase-field simulations.

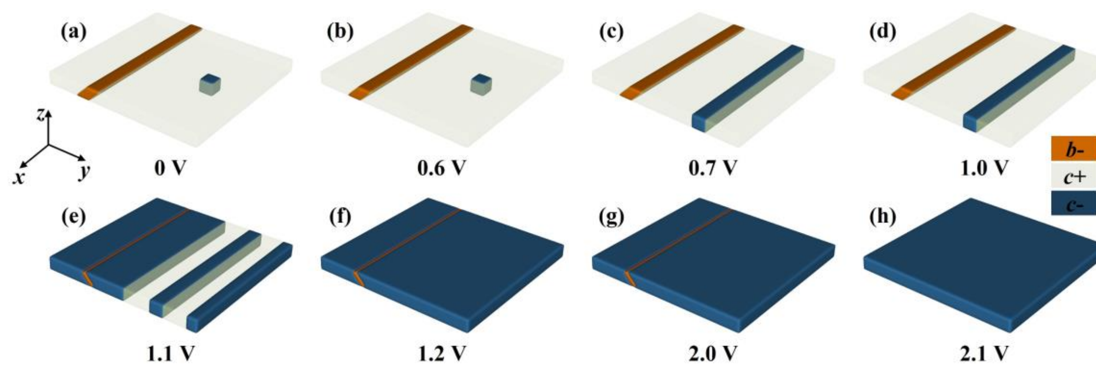

Fig. 2 | Evolution of pre-existing ferroelectric domain structure with increasing applied voltage in the HZO film with 128 nm (length) ×128 nm (width) × 10 nm (thickness) via phase-field simulations. a The initial domain configuration consists of a *b*- domain and a *c*- domain embedded within a *c*+ domain. The sequential evolution of domain structures under gradually increasing applied voltage by a voltage step of 0.1 V: **b** 0.6 V, **c** 0.7 V, **d** 1.0 V, **e** 1.1 V, **f** 1.2 V, **g** 2.0 V, and **h** 2.1 V. The region corresponding to the *c*+ domain is rendered semi-transparent to enhance the visual clarity of the domain evolution process.

ARTICLE

ARTICLE IN PRESS

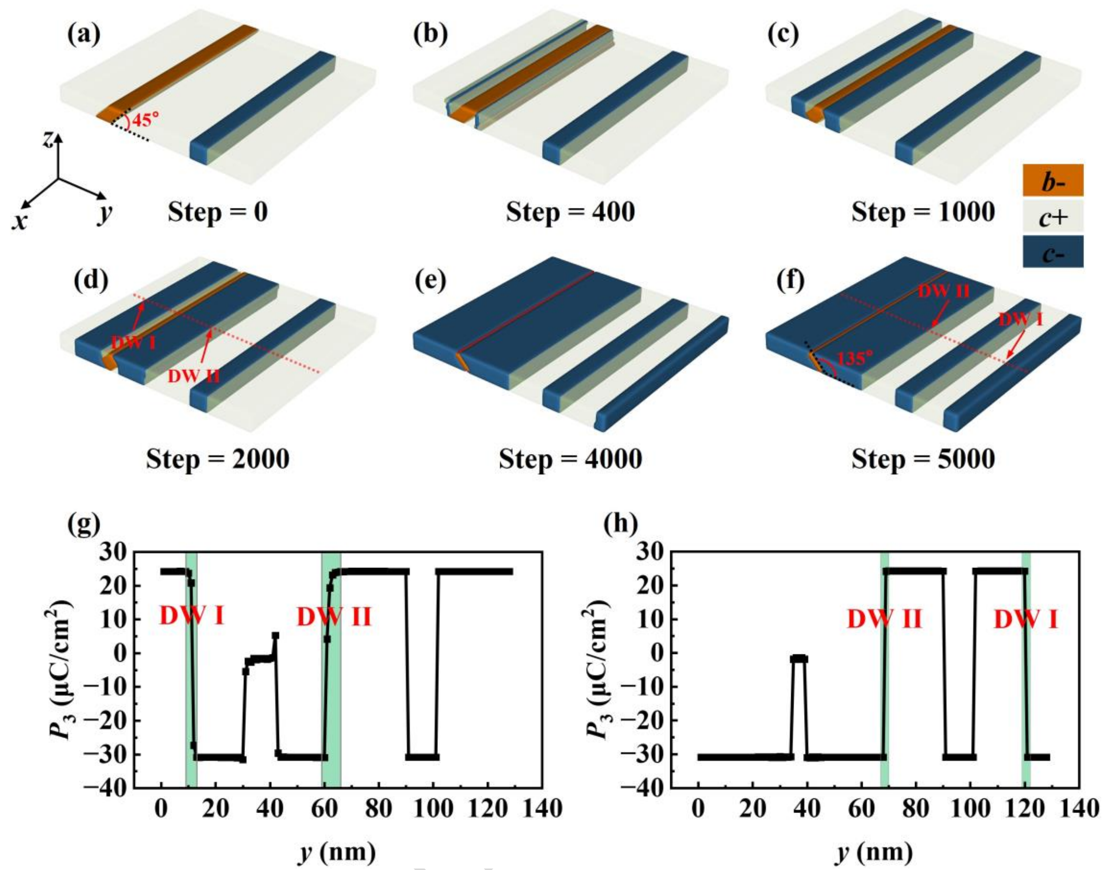

Fig. 3 | Dynamic evolution of the domain structure under an applied voltage of 1.1 V. a The initial domain structure from the equilibrium state of Fig. 2d under an applied voltage of 1.0 V. Temporal evolution of the domain structure at different time steps: **b** 400, **c** 1000, **d** 2000, **e** 4000, and **f** 5000. The distributions of P_3 along the *y* direction at time steps **g** 2000 and **h** 5000, corresponding to the red dashed lines in **d** and **f**, respectively. For clarity, the *c*+ domain regions are rendered semi-transparent to illustrate the domain evolution.

ARTICLE

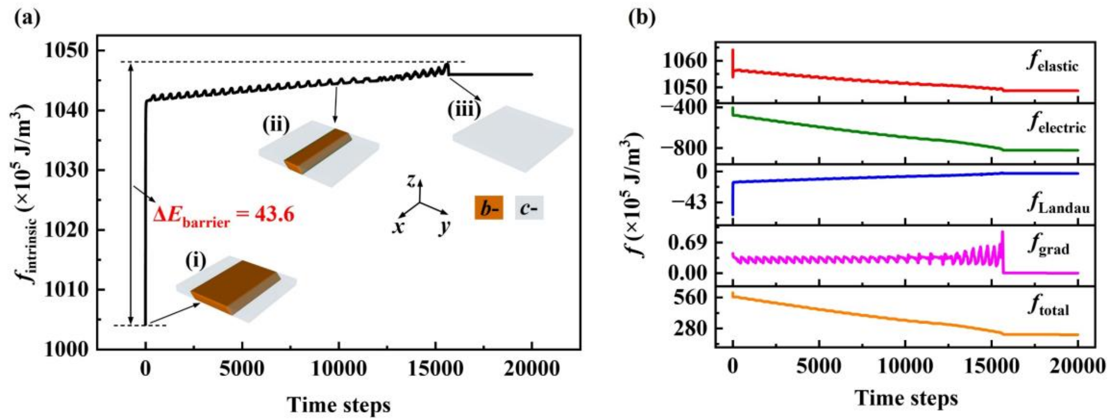

Fig. 4 | Energy barrier analysis of 90° DW migration. a Evolution of the intrinsic energy density (namely, subtracting electrostatic energy density from total energy density) as a function of time steps. The insets show the corresponding domain structures at different time steps: (i) 0, (ii) 10,000, and (iii) 16,000. **b** Evolution of each energy component density and the total energy density with time steps.

ARTICLE IN PRESS

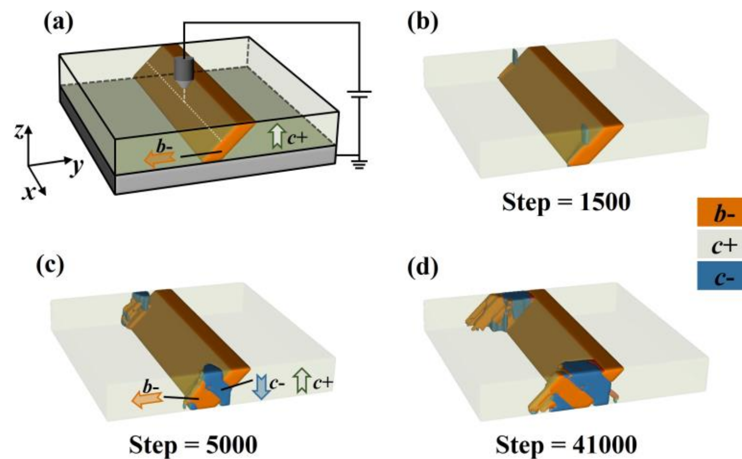

Fig. 5 | Effect of 90° DWs on local 180° polarization switching in the HZO film with 128 nm (length) ×128 nm (width) × 20 nm (thickness) under a Lorentz-like probe voltage. a The initial domain configuration consists of a *b*- domain embedded within a *c*+ domain. Temporal evolution

ARTICLE IN PRESS

of the domain structure under $\phi_0 = 1.9$ V at different time steps: **b** 1500, **c** 5000, and **d** 41,000. For clarity in visualizing the domain evolution, the images in **b-d** are translated along the x axis so that the probe center is located at $x = 0$, and regions corresponding to the $c+$ domain are rendered as semi-transparent.

ARTICLE IN PRESS